NANO LETTERS

Letter

pubs.acs.org/NanoLett

Rashba Effect in a Single Colloidal $CsPbBr_3$ Perovskite Nanocrystal Detected by Magneto-Optical Measurements

Maya Isarov,[†] Liang Z. Tan,[‡] Maryna I. Bodnarchuk,[§,∥] Maksym V. Kovalenko,[*,§,∥] Andrew M. Rappe,[*,‡] and Efrat Lifshitz[*,†]

[†]Schulich Faculty of Chemistry, Nancy and Stephen Grand Technion Energy Program, Russell Berrie Nanotechnology Institute, Solid State Institute, Technion, Haifa 3200003, Israel

[‡]Department of Chemistry, University of Pennsylvania, Philadelphia, Pennsylvania 19104-6323, United States

[§]Institute of Inorganic Chemistry, Department of Chemistry and Applied Biosciences, ETH Zürich, Vladimir Prelog Weg 1, CH-8093 Zürich, Switzerland

[∥]Laboratory for Thin Films and Photovoltaics, Empa − Swiss Federal Laboratories for Materials Science and Technology, Überlandstrasse 129, CH-8600 Dübendorf, Switzerland

Supporting Information

ABSTRACT: This study depicts the influence of the Rashba effect on the band-edge exciton processes in all-inorganic $CsPbBr_3$ perovskite single colloidal nanocrystal (NC). The study is based on magneto-optical measurements carried out at cryogenic temperatures under various magnetic field strengths in which discrete excitonic transitions were detected by linearly and circularly polarized measurements. Interestingly, the experiments show a nonlinear energy splitting between polarized transitions versus magnetic field strength, indicating a crossover between a Rashba effect (at the lowest fields) to a Zeeman effect at fields above 4 T. We postulate that the Rashba effect emanates from a lattice distortion induced by the Cs^+ motion degree of freedom or due to a surface effect in nanoscale NCs. The unusual magneto-optical properties shown here underscore the importance of the Rashba effect in the implementation of such perovskite materials in various optical and spin-based devices.

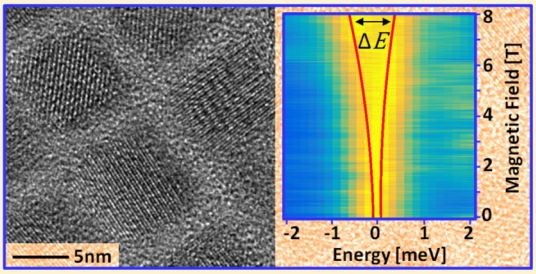

KEYWORDS: *Metal halide perovskite, nanocrystal, Rashba spin−orbit coupling, magneto-optics*

The halide perovskites of the type AMX_3 (A = organic molecules or inorganic ions; M = Pb, Sn; X = Cl, Br, I) are in the forefront of current interest, having re-emerged after the groundbreaking recent discovery of their effectiveness in photovoltaic cells.[1−12] This stimulus caused a renaissance of exploration of new intriguing physical phenomena with potential prospects in a variety of applications including light-emitting diodes,[13−16] lasers,[17−19] single photon sources,[20−22] photodetectors,[23] γ-ray detectors,[24] and spintronic devices.[25,26] The spin degree of freedom and in particular the Rashba effect have attracted much attention in these materials.[27−31] The existence of the Rashba effect in $CsPbBr_3$ nanocrystals and its manifestation in the optical properties is the subject of this work.

The AMX_3 materials are composed of interconnected $[MX_6]^{-4}$ octahedral units, forming a 3D network with cuboctahedral voids that accommodate organic/inorganic ions (e.g., methylammonium [MA], formamidinium [FA]; Cs^+).[35−38] Such perovskite lattices often undergo various structural distortion or even phase transitions to lower-symmetry polymorphs upon application of an external perturbation (e.g., temperature or pressure).[39−45] The various phases of AMX_3 perovskites exhibit an unusual combination of optical and electronic properties, including large optical absorption coefficient[46,47] with long carrier diffusion lengths (up to microns).[48−51] Furthermore, perovskite materials show interesting excitonic properties,[52−58] including suggestions of anomalous spin effects.[27−29]

The electronic band structure near the band gap is mainly composed of M and X atomic orbitals:[59−64] the conduction band edge is based on M orbitals with p angular momentum character, while the valence band edge includes X p-orbitals combined with M s-orbital contribution. The heavy metal (e.g., Pb) contribution to the conduction band induces strong spin−orbit coupling (SOC), which lifts the degeneracy of the sextet p manifold (including spin) into doublet (J = 1/2) and quartet (J = 3/2) submanifolds. Hence, a band-edge optical absorption at a symmetric point at the Brillouin zone involves a transition from valence-band state with an angular momentum $J_h = S_h$ = 1/2 (projection on z, $m_S = \pm 1/2$) to the split-off conduction-band state with J_e = 1/2 ($m_J = \pm 1/2$). A single exciton (X) recombination related to the $S_h \leftrightarrow J_e$ transition is anticipated to have a structural symmetry dependence.[65,66] This involves a

Received: May 28, 2017
Published: June 28, 2017

DOI: 10.1021/acs.nanolett.7b02248
Nano Lett. 2017, 17, 5020−5026

splitting into a dark singlet ($J_x = 0$) and a degenerate bright triplet ($J_x = 1$, $m_J = \pm 1,0$) states in a cubic structure, and a further lifting of degeneracy in phases with lower symmetry or under induced distortion.

Although the $[PbX_6]^{-4}$ network dominates the electronic band structure, the A-site ions have special impact on the physical properties, due to their vibrational degrees of freedom. The polar organic ions (e.g., MA or FA) form hydrogen bonds to the halide anions,[67,68] and thus their motion induces displacement of the X and M ions.[69] Hydrogen bond breaking at elevated temperatures permits freer rotation of the organic A^+ ions, toward coherent alignment.[67,70−77] Similarly, displacive freedom of a relatively small inorganic ion like Cs^+ within the cuboctahedral void may induce a net polarization.[78] In addition, the M^{+2} (e.g., Sn, Pb) s^2 lone pair can be stereochemically active and able to induce a local symmetry breaking within the $[MX_6]^{-4}$ cage (see SI).[79,80] All these atomic and orbital displacements create crystalline distortion, which can lead to (local or global) inversion-symmetry breaking and/or a buildup of local polarization;[67−69,72−80] when inversion symmetry breaking is combined with SOC, it gives the so-called Rashba effect.[30−32,81,82]

Rashba and Dresselhaus effects split the electronic bands in crystals with SOC that lack inversion symmetry, giving pairs of bands with counter-propagating spin directions.[83,84] While a coexistence of Rashba and Dresselhaus effects is expected to be present in $FASnI_3$,[33] theoretical investigations[29−32,34,62] predict only the Rashba effect in lead halide perovskites. Therefore, the current work focuses on the Rashba effect. Despite a long history of Rashba effect research in various materials and investigations of various physical aspects of halide perovskites,[75] experimental evidence linking the two has only recently appeared in $MAPbI_3$[85] and in the angle-resolved photoelectron spectroscopy measurements of $MAPbBr_3$.[86] Theoretical predictions have suggested that the Rashba effect suppresses carrier recombination in the halide perovskites by making the band-edge transitions spin- or momentum-forbidden.[25,30,31]

The current work investigates the interplay of Rashba and band-edge excitonic effects in $CsPbBr_3$ single colloidal nanocrystals (NCs) in particular showing evidence for the Rashba effect in the excitonic magneto-photoluminescence spectra of $CsPbBr_3$ at low temperatures. This study investigates the band-edge excitonic transitions by measuring the linearly and circularly polarized photoluminescence of a single particle under an applied magnetic field. The experiments resolve discrete narrow excitonic transitions with an energy splitting that increases nonlinearly with the magnetic field strength. The nonlinearity in the exciton photoluminescence (PL) splitting observed in the experiment is supported by our theoretical calculations, suggesting a crossover between the Rashba effect at low magnetic fields to a Zeeman effect at higher fields.

The all-inorganic bromide perovskite $CsPbBr_3$ was selected for the current study due to its relative chemical and photochemical stability,[2,8,87] and facile access to cubic-shaped, monodisperse NCs via colloidal synthesis.[1,3,88,89] The $CsPbBr_3$ NCs under consideration were synthesized using an established procedure,[1,3] possess an orthorhombic crystallographic structure (space group *Pnma*, 62), and have sizes of 9.5 ± 0.1 nm; see transmission electron microscopy (TEM) images in the Supporting Information (SI), Figure S1 and a variable temperature X-ray diffraction observation as reported in ref 90. The magneto-optical properties of a single NC of $CsPbBr_3$ were detected by immersing them in a magneto-cryogenic system, when mounted on a confocal fiber-based probe with a submicron excitation spot, referred to as micro-PL (μ-PL). For further details, see a description in the SI. The excitation power was <50 $W \cdot cm^{-2}$, ensuring the generation of single excitons (see SI, Figure S2). Figure 1a displays a set of reflectance

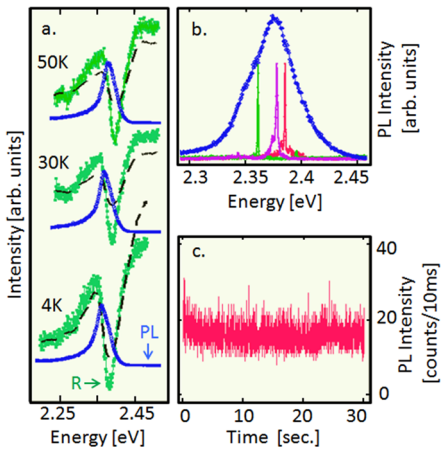

Figure 1. (a) Reflectance (R) and PL spectra of ensemble of $CsPbBr_3$ NCs. The black dashed curves are fit to the reflectivity spectra, with exciton peak energy (E_x) 2.365 eV at 4.2 K, 2.371 eV at 30 K, and 2.38 eV at 50 K. (b) μ-PL spectra of three individual NCs and broad emission (blue curve) of an ensemble of NCs. (c) Intensity trace of representative μ-PL of a single NC.

(green curves) and PL spectra (blue curves) of an ensemble of NCs, monitored near the band edge and recorded at various temperatures. The reflectance spectra are dominated by dispersive signals overlapped by the emission high-energy side tails. The reflectance curves have been fitted to the real part of a linear susceptibility according to the Kramers−Kronig relation, $R(E) = R_0 + R_x \cdot \mathcal{R}\left(\frac{E_x - E + i\Gamma_x}{\Gamma_x^2 + (E - E_x)^2}\right)$ (see black dashed curves), where R_0 is the background, R_x is the amplitude, E_x is the resonance energy (viz., band gap energy), and Γ_x is the broadening parameter.[91] The emission spectra are ascribed to exciton transitions with extensive interpretation provided below. It is seen from Figure 1a that the reflectance and emission spectra both show a shift to higher energy ("blue shift") with an increase of the temperature, which is in contradiction to the behavior of many II−VI and III−V compound semiconductors but is often found in group IV elemental semiconductors.[43,58,92,93] The PL Stokes shift is positive and ranges from 4−7 meV at low temperatures (4.2−50 K). The exciton lifetime was monitored by following a PL-decay curve (Figure S3), revealing a change of the lifetime from 0.5 to 20 ns with the increase of the temperature from 4.2 K to room temperature. The observed lifetime is compatible with the most recent reports.[21−23]

In order to validate the rich physical phenomena in $CsPbBr_3$, the magneto-optical experiment discussed below solely focuses on a single NC at 4.2 K. Figure 1b presents μ-PL spectra of three individual NCs, characterized by sharp bands (with full width at half-maximum [fwhm] ∼0.9 meV) and weak subsidiary bands. The spectra from individual NCs are compared with that of an ensemble (see blue curve in Figure 1b), illustrating the superior spectral resolution when monitoring an individual NC (limited by the experimental resolution of 0.4 meV). Additional observations of single NC μ-

DOI: 10.1021/acs.nanolett.7b02248
Nano Lett. 2017, 17, 5020−5026

PL spectra are shown in Figure S4. Furthermore, Figure 1c exhibits an intensity trace of a representative μ-PL sharp band shown in Figure 1b, showing only small jitter around the mean peak intensity without "off" times, suggesting blinking-free exciton recombination. The time-traces of the NCs were examined with and without magnetic field. Additional traces beyond Figure 1c are shown in Figure S5, presenting spectral stability under magnetic field. The blinking-free behavior is in agreement with a recent report on $CsPbCl_xBr_{3-x}$,[20] and $CsPbBr_3$,[94] but in contradiction to cases that showed pronounced fluorescence intermittencies in iodide and bromide perovskites, resembling the blinking phenomenon in three-dimensional colloidal quantum dots.[21,22]

Figure 2a,b shows unpolarized μ-PL spectra of two different single $CsPbBr_3$ NCs, recorded with and without a magnetic field (B), as labeled in the panel. The spectra at B = 0 T include a dominant band associated with the band-edge exciton recombination, which together with weak shoulders at the low- and high-energy tails are marked as spectral regime I. Also, the μ-PL spectra contain one or more broad peaks blue-shifted by 2.3 meV (labeled as regime II) and 5.7 meV (labeled as regime III) from that of the exciton peak. The exciton band in regime I was best fit by two Lorentzian functions after subtracting their shoulders (see SI, Figure S6) with an interpeak energy gap that varies from one NC to another from 0.2 to 0.4 meV at B = 0 T. The energy gap increases with B strength, up to 1.3 meV at 8 T. Figure 2c displays a statistical analysis of 1500 spectral scans of one NC, "Dot 1", by plotting the Lorentzian functions' maxima versus B (colored symbols). A fit to the experimental points is shown by the solid lines, which clearly reveals the existence of an energy split at 0 T. This is not compatible with a fit with a vanishing gap at B = 0 T (dashed lines). Lorentzian deconvolution of excitons in other NCs are shown at the SI, Figures S7, further supporting the existence of energy split at B = 0 T. Figure 2d displays a plot of the peak splitting energy gap, ΔE, of the unpolarized exciton of "Dot 2" versus B (red squares). It is evident from Figure 2d that the splitting cannot be fitted to a linear Zeeman function (green curve) and neither to a quadratic Zeeman function (blue curve) according to equations given in refs 95 and 96. Additional attempts to implement a normal and anomalous Zeeman fit (see SI, Figure S8) showed a large deviation from experiment. Hence, the two peaks resolved by the Lorentzian deconvolution, persisting even at vanishing magnetic field and the nonlinear dependence on B, are at odds with a Zeeman mechanism. The presented theoretical calculation below, which considers both the Zeeman and Rashba terms, does explain the observed nonlinear dependence of the PL splitting versus magnetic field, as well as the nonvanishing energy split at B = 0 T (black circles in Figure 2d). Detailed elaboration of the combined Rashba and Zeeman model is discussed below and in the SI.

To understand the character of the splitting of the exciton band, we record linearly polarized spectra under the influence of a magnetic field of 8 T, excited by unpolarized and off-resonant light, as shown for Dot 1 in Figure 3a. The emission

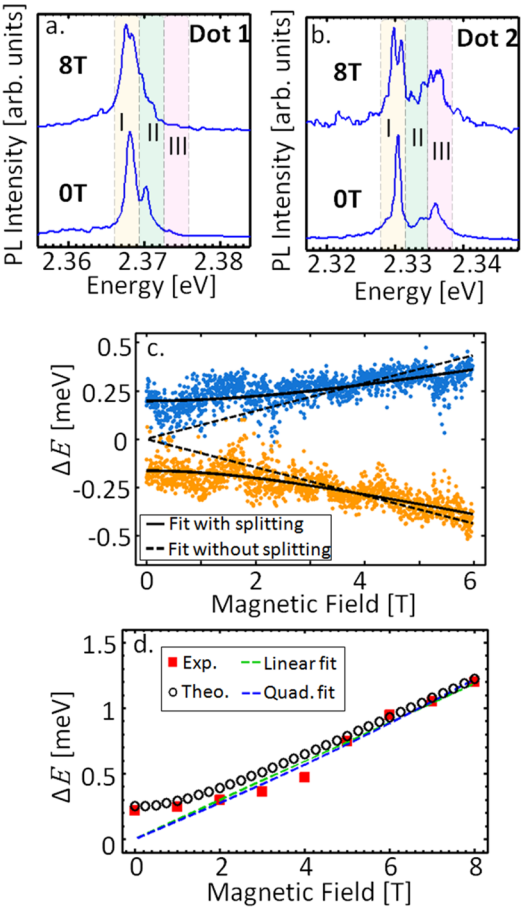

Figure 2. (a,b) Unpolarized μ-PL spectra (blue curves) of two different $CsPbBr_3$ single NCs, recorded at B = 0 and B = 8 T at 4.2 K. The spectra are divided into three regimes I, II, and III, as discussed in the text. (c) Plot of the major band split-component energy (collected from 1500 different μ-PL scans of Dot 1) versus strength of a magnetic field (colored dots represent fits to experimental spectral peaks at one B field value, the black line is the best fit as a function of B, while the dashed lines are attempts to fit the data with a zero split at B = 0 T. (d) Plot of energy split, ΔE, of an exciton band in regime I (red squares) versus magnetic field strength for Dot 2. Green and blue lines are fits to linear and quadratic Zeeman equations, respectively. The black circles correspond to theoretical calculations including Rashba Zeeman interactions.

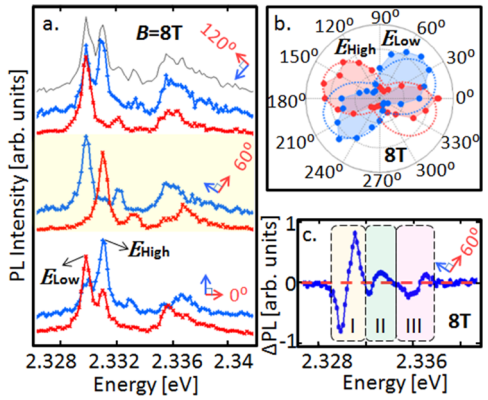

Figure 3. (a) Orthogonal linearly polarized μ-PL split components (red/blue curves) of a single NC, recorded at B = 8 T, excited by unpolarized and off-resonant light. The detected linear polarization axes are indicated by orthogonal arrows. The black curve is unpolarized detection. (b) Polar plot of the exciton band as in panel (a), showing polarization dependence of high-energy (E_{High}) and low-energy (E_{Low}) peaks, respectively. The dashed lines show the theoretical linear polarization dependence, calculated from the exciton model (see text). (c) PL difference spectrum of the 60°/150° orthogonal linear polarizations shown in panel (a).

DOI: 10.1021/acs.nanolett.7b02248
Nano Lett. 2017, 17, 5020−5026

beam is detected with a linear polarizer, rotated between two orthogonal orientations (red and blue curves) with respect to a laboratory axis (angles are marked as insets). The corresponding unpolarized spectrum is shown by a black curve, and it is the sum of each pair of orthogonal components (top/middle/bottom spectra in Figure 3a). The blue and red curves are nearly completely nonoverlapping and show the greatest contrast at a specific orthogonal position of 60°/150° (middle spectra), probably due to coincident alignment of one unique crystallographic axis with the direction of B. Figure 3b displays a polar plot of the split exciton band in spectral regime I, recorded at 8 T. This plot shows two nearly orthogonal open-eight shapes, where the colored symbols corresponding to the high-energy (E_{High}) and low-energy (E_{Low}) bands as marked in panel a and the dashed line refers to the theoretical simulation as discussed below. A figure-eight shape represents a linear polarization behavior; however, deviation from a perfect figure-eight and perfect orthogonality suggest the existence of elliptical polarization rather than pure linear polarization (see discussion below). Figure 3c displays a difference spectrum of the 60°/150° components from panel a, emphasizing the (nearly) full polarization. A careful look at this difference exposes inter-relationships among bands. Examination of the three different spectral regimes (labeled I, II, and III in Figure 2b) highlights positive and negative pairs in each regime. While the predominant band in regime I is assigned to an exciton transition, the polarization correlation of regimes II and III with that of I resembles a behavior of either phonon-replica as anti-Stokes lines, decay from forbidden states or excited-state excitons. Excited-state excitons are unlikely due to the low power of the excitation. Polarized transition from dark states (more likely with an angular momentum of $J_x = 0$) are also unexpected (see below). The occurrence of a phonon anti-Stokes transitions is a plausible process, however the discussion about it is provided later in the manuscript. Here, we mainly focus the discussion on the ground-state excitonic transitions (spectral regime I).

At this point we proposed that the exciton split components shown in Figure 2a are related to the bright exciton $m_x = \pm 1$ emission, where the linear polarization characteristic (shown in Figure 3a) is associated with the linear recombination of the projections, m_J. The deviation from a pure linear polarization (shown by the polar plot in Figure 3b) may originate from a shape distortion, which induces considerable mixing with nearby dark states (e.g. $J_x = 0$, $m_x = 0$, or $J_x = 1$, $m_x = 0$). This hypothesis will be further elaborated below. Similar assignment to band-edge polarized transitions was most recently given in ref 94, published during the process of reviewing the present work.

Figure 4a presents a set of μ-PL spectra of a single NC, excited by unpolarized light, and detected via left and right circular polarizers (a combination of quarter-wave plate and linear polarizer). Comparable to the unpolarized and linearly polarized spectra, the evolution of each circular component in regime I shows a splitting into high-energy (E_{High}) and low-energy (E_{Low}) bands, related to a recombination of the $J_x = 1$, $m_x = \pm 1$ bright excitons. In fact, the E_{Low} component has a very weak dependence on B, supposedly due to the influence of a nearby $J_x = 1$, $m_x = 0$ state, spaced apart by ~1 meV (see theoretical model at the SI). The circular polarization of regimes II and III have a correlation to that of regime I (not shown here), in a similar manner to the behavior found in the linearly polarized spectra (Figure 3c). Overall, the coexistence

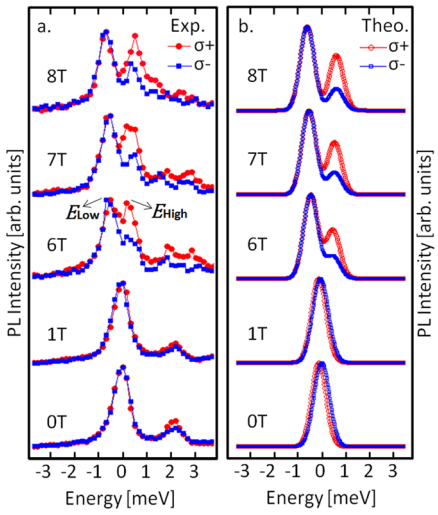

Figure 4. (a) μ-PL spectra of a single NC, excited by unpolarized light but detected with left and right circular polarizations. (b) Calculated PL spectra from exciton model for right-polarized (σ^+) and left-polarized (σ^-) light.

of both linear and circular polarization of the same optical transitions up to the highest measured magnetic field, as was shown in Figures 3 and 4, indicates the presence of elliptical polarization. As will be discussed below, the deviation from a pure polarization is related to a centrosymmetry breaking which consequently leads to state mixing with nearby dark states.

To understand the experimental observations, we develop a model for excitonic PL in $CsPbBr_3$, taking into account Rashba and magnetic-field effects. We write the Hamiltonian for the exciton relative coordinate (r) degree of freedom as

$$H = -\frac{\vec{\nabla}_r^2}{2m_r} + V(r) + (\alpha_e\vec{\sigma}_e - \alpha_h\vec{\sigma}_h)(\hat{n} \times i\vec{\nabla}_r) + \frac{1}{2}\mu_B\vec{B}(g_e\vec{\sigma}_e - g_h\vec{\sigma}_h) \quad (1)$$

Here, $V(r)$ is the electron−hole interaction, m_r is the reduced mass, α_e and α_h are Rashba coefficients for electron and hole, respectively, and g_e and g_h are g-factors for electron and hole, respectively.

The spin degrees of freedom in the conduction-band manifold ($m_J = \pm 1/2$) and valence-band manifold ($m_S = \pm 1/2$) states are represented by the Pauli matrices, $\vec{\sigma}_e$ and $\vec{\sigma}_h$, respectively. As the orthorhombic phase of $CsPbBr_3$ possesses inversion symmetry, symmetry breaking arises mainly by a surface effect or due to a lattice distortion induced by the Cs^+ motion normal to a surface.[78,80] Hence, inversion symmetry breaking combined with internal spin−orbit coupling in these compounds satisfies the conditions for the Rashba effect. The surface normal is denoted by $\hat{n}$ in eq 1. A detailed derivation of this Hamiltonian is given in the SI. In the following, we have used Rashba parameters of $\alpha_e = 0.2$ eV·Å and $\alpha_h = 0.05$ eV·Å. The valence-band Rashba parameter is expected to be smaller than the conduction-band Rashba parameter, as suggested by DFT calculations on halide perovskite tetragonal phases.[29] We have fixed the g-factors to be $g_e = 1.6$ and $g_h = 0.8$, which are in fair agreement with the total effective g-factor of $g_{eff} = 2.3$ measured under high magnetic fields,[55] as well as the g-factor difference $\Delta g = 0.65$ measured in ref 27.

We numerically solve eq 1 for excitonic energy levels, using a localized basis set for the relative coordinate degree of freedom. We calculate PL spectra from the solutions of our exciton

DOI: 10.1021/acs.nanolett.7b02248
Nano Lett. 2017, 17, 5020−5026

model and optical matrix elements. The calculated circularly polarized spectra are depicted in Figure 4b, following the color scheme of Figure 4a. The model and experiment match closely, when elliptical polarization consistent with the experimental spectra is used. The calculated PL spectra show that the splitting of the PL peak is small for $B < 4$ T, and increases rapidly above 4 T. This trend is also observed in our experimental spectra (Figures 2b and 4a). Linearly polarized spectra calculated from this exciton model are in a good agreement with experiment (see a fit to the polar plot in Figure 3b by the dashed lines). The calculated circularly polarized spectra (Figure 4b) show that, at large magnetic fields (8 T), each PL peak contains both right- and left- polarized components related to the $J_x = 1$, $m_x = \pm 1$ components. The observation seen in the experimental circularly polarized spectra (Figure 4a) is a result of elliptical polarization. In other words, it results from the breaking of the perfect circular polarization selection rules observed in bulk $CsPbBr_3$ at high magnetic fields.[55] We attribute this elliptically polarized exciton emission to strong centrosymmetry breaking due to a distortion normal to the surface or due to the surface itself, as well as to an induced mixing with nearby dark states. The high-energy and low-energy peaks in Figure 4a contain different ratios of left- and right-pol E_{Low} transition experiences mixing with close by dark state. This effect is captured in our model by using asymmetric transition dipole matrix elements (see SI).

Because of the coexistence of Rashba and Zeeman terms in eq 1, the exciton wave functions are in general not eigenstates of $\vec{\sigma}_e$ and $\vec{\sigma}_h$ but are mixtures of different electron and hole spin states. At large magnetic fields, the Zeeman term dominates and the splitting of bright exciton levels displays a linear magnetic field dependence, as reported by Galkowski et al.[55] In this regime, the electron and hole spins are aligned (anti)parallel to the magnetic field. On the other hand, the Rashba term dominates at $B \approx 0$. In this limit, the exciton eigenstates are instead singlet and triplet combinations of electron and hole spins. The spin−orbit coupling responsible for the Rashba effect causes a splitting between the singlet and triplet states, resulting in the $B = 0$ splitting seen in Figures 2c and 2d. Therefore, a crossover between Rashba and Zeeman physics is expected to occur at intermediate magnetic fields. An order of magnitude estimate for the crossover magnetic field is when the Zeeman splitting energy is equal to the singlet−triplet splitting caused by the Rashba effect: $\left(\frac{1}{2}\right)g\mu_B B \approx (\alpha/a_0)^2/\Delta E_b$, where a_0 is the exciton Bohr radius and ΔE_b is the difference in binding energy of the excitons with s and p envelope functions (see SI). Taken together, the existence of two distinct peaks in the zero magnetic-field spectra and the nonlinearity in the exciton PL splitting observed in the experiment and in our theory (Figure 2c) are signs of the Rashba effect in these NCs.

It should be noted that a recent paper exploring the influence of optical properties at giant magnetic fields (up to 100 T) excluded the contribution of Rashba effect.[55] Our work is performed at a very fine spectral resolution under much lower magnetic-field strengths. There is likely no contradiction between these experimental efforts, as we expect the Rashba effect to be negligible compared to the Zeeman term under the strong magnetic fields of ref 55.

Given the preceding discussion of the Rashba effect, we return to the observation of the anti-Stokes side-bands (Figure 3). The energies of these side-bands are shifted from the main exciton band by 2.3 and 5.7 meV. These energies correlate well with Cs^+ polar phonon modes identified by Raman spectroscopy and DFT calculations.[78,97,98] The circumstance for the appearance of pronounced anti-Stokes bands over the Stokes bands is possibly related to the structural distortions induced by illumination, resulting in nonthermal phonon populations which could change the relative weights of Stokes/anti-Stokes bands. Given the complexity of this mechanism, which involves dynamical, excitonic, and spin degrees of freedom, we defer a detailed investigation to a future publication.

In conclusion, we have presented magneto-PL spectra of single nanocrystals of $CsPbBr_3$ in magnetic fields up to 8 T. The improved resolution afforded by these single nanocrystal measurements has allowed for the observation of a crossover between Rashba and Zeeman physics in this system, providing the first experimental proof of Rashba effects on the PL spectra of a halide perovskite. We demonstrate analytically and numerically that a model incorporating Rashba and Zeeman physics can reproduce the observed B field dependence and polarization dependence of exciton emission spectra. By showing that excitonic properties are strongly affected by the Rashba effect, this work has advanced the understanding of the spin−orbit and Rashba effects in the photovoltaic properties of the halide perovskites.

■ ASSOCIATED CONTENT

Supporting Information

The Supporting Information is available free of charge on the ACS Publications website at DOI: 10.1021/acs.nanolett.7b02248.

Synthesis and magneto-optical measurement details, calculations, and additional figures. (PDF)

■ AUTHOR INFORMATION

Corresponding Authors

*E-mail: (A.M.R.) rappe@sas.upenn.edu.
*E-mail: (M.K.) mvkovalenko@ethz.ch.
*E-mail: (E.L.) ssefrat@technion.ac.il.

ORCID

Liang Z. Tan: 0000-0003-4724-6369
Maksym V. Kovalenko: 0000-0002-6396-8938
Andrew M. Rappe: 0000-0003-4620-6496
Efrat Lifshitz: 0000-0001-7387-7821

Author Contributions

The manuscript was prepared through the contribution of all coauthors. All authors have given approval to the final version of the manuscript. M.I. and L.Z.T. contributed equally to this work.

Notes

The authors declare no competing financial interest.

■ ACKNOWLEDGMENTS

M.I. expresses her gratitude to the fellowship received by the Nancy and Stephen Grand Technion Energy Program. M.I. and E.L. thank the support of the Volkswagen Stiftung (Project No. 88116), the Israel Science Foundation (Project No. 1508/14 and 914/15), and the European Commission via the Marie-Sklodowska Curie action Phonsi (H2020-MSCA-ITN-642656). L.Z.T. and A.M.R. acknowledge the support of the Office of Naval Research under Grant N00014-17-1-2574 and computational support from the High-Performance Computing Modernization Office of the Department of Defense. M.I.B.

DOI: 10.1021/acs.nanolett.7b02248
Nano Lett. 2017, 17, 5020−5026

acknowledges financial support from the Swiss National Science Foundation (SNF Ambizione Project ZENP2_154287). M.V.K. is grateful to European Union (ERC Starting Grant NANOSOLID, GA 306733).

REFERENCES

(1) Protesescu, L.; Yakunin, S.; Bodnarchuk, M. I.; Krieg, F.; Caputo, R.; Hendon, C. H.; Yang, R. X.; Walsh, A.; Kovalenko, M. V. *Nano Lett.* **2015**, *15*, 3692−3696.
(2) Kulbak, M.; Gupta, S.; Kedem, N.; Levine, I.; Bendikov, T.; Hodes, G.; Cahen, D. *J. Phys. Chem. Lett.* **2016**, *7*, 167−172.
(3) Cottingham, P.; Brutchey, R. L. *Chem. Commun.* **2016**, *52*, 5246−5249.
(4) Grätzel, M. *Nat. Mater.* **2014**, *13*, 838−842.
(5) Beal, R. E.; Slotcavage, D. J.; Leijtens, T.; Bowring, A. R.; Belisle, R. A.; Nguyen, W. H.; Burkhard, G. F.; Hoke, E. T.; McGehee, M. D. *J. Phys. Chem. Lett.* **2016**, *7*, 746−751.
(6) Brenner, T. M.; Egger, D. A.; Kronik, L.; Hodes, G.; Cahen, D. *Nat. Rev. Mater.* **2016**, *1*, 15007.
(7) Klein-Kedem, N.; Cahen, D.; Hodes, G. *Acc. Chem. Res.* **2016**, *49*, 347−354.
(8) Zuo, C.; Bolink, H. J.; Han, H.; Huang, J.; Cahen, D.; Ding, L. *Adv. Sci.* **2016**, *3*, 1500324.
(9) Egger, D. A.; Rappe, A. M.; Kronik, L. *Acc. Chem. Res.* **2016**, *49*, 573−581.
(10) Heo, J. H.; Im, S. H.; Noh, J. H.; Mandal, T. N.; Lim, C. S.; Chang, J. A.; Lee, Y. H.; Kim, H. J.; Sarkar, A.; Nazeeruddin, M. K.; Grätzel, M. *Nat. Photonics* **2013**, *7*, 486−491.
(11) Giorgi, G.; Fujisawa, J. I.; Segawa, H.; Yamashita, K. *J. Phys. Chem. Lett.* **2013**, *4*, 4213−4216.
(12) Dastidar, S.; Egger, D. A.; Tan, L. Z.; Cromer, S. B.; Dillon, A. D.; Liu, S.; Kronik, L.; Rappe, A. M.; Fafarman, A. T. *Nano Lett.* **2016**, *16*, 3563−3570.
(13) Kulbak, M.; Cahen, D.; Hodes, G. *J. Phys. Chem. Lett.* **2015**, *6*, 2452−2456.
(14) Song, J.; Li, J.; Li, X.; Xu, L.; Dong, Y.; Zeng, H. *Adv. Mater.* **2015**, *27*, 7162−7167.
(15) Yassitepe, E.; Yang, Z.; Voznyy, O.; Kim, Y.; Walters, G.; Castañeda, J. A.; Kanjanaboos, P.; Yuan, M.; Gong, X.; Fan, F.; Pan, J.; Hoogland, S.; Comin, R.; Bakr, O. M.; Padilha, L. A.; Nogueira, A. F.; Sargent, E. H. *Adv. Funct. Mater.* **2016**, *26*, 8757.
(16) Meyns, M.; Perálvarez, M.; Heuer-Jungemann, A.; Hertog, W.; Ibáñez, M.; Nafria, R.; Genç, A.; Arbiol, J.; Kovalenko, M. V.; Carreras, J.; Cabot, A. *ACS Appl. Mater. Interfaces* **2016**, *8*, 19579−19586.
(17) Yakunin, S.; Protesescu, L.; Krieg, F.; Bodnarchuk, M. I.; Nedelcu, G.; Humer, M.; De Luca, G.; Fiebig, M.; Heiss, W.; Kovalenko, M. V. *Nat. Commun.* **2015**, *6*, 8056.
(18) Fu, Y.; Zhu, H.; Schrader, A. W.; Liang, D.; Ding, Q.; Joshi, P.; Hwang, L.; Zhu, X. Y.; Jin, S. *Nano Lett.* **2016**, *16*, 1000−1008.
(19) Tang, X.; Hu, Z.; Chen, W.; Xing, X.; Zang, Z.; Hu, W.; Qiu, J.; Du, J.; Leng, Y.; Jiang, X.; Mai, L. *Nano Energy* **2016**, *28*, 462−468.
(20) Rainò, G.; Nedelcu, G.; Protesescu, L.; Bodnarchuk, M. I.; Kovalenko, M. V.; Mahrt, R. F.; Stöferle, T. *ACS Nano* **2016**, *10*, 2485−2490.
(21) Hu, F.; Zhang, H.; Sun, C.; Yin, C.; Lv, B.; Zhang, C.; Yu, W. W.; Wang, X.; Zhang, Y.; Xiao, M. *ACS Nano* **2015**, *9*, 12410−12416.
(22) Park, Y. S.; Guo, S.; Makarov, N. S.; Klimov, V. I. *ACS Nano* **2015**, *9*, 10386−10393.
(23) Ramasamy, P.; Lim, D. H.; Kim, B.; Lee, S. H.; Lee, M. S.; Lee, J. S. *Chem. Commun.* **2016**, *52*, 2067−2070.
(24) Yakunin, S.; Dirin, D. N.; Shynkarenko, Y.; Morad, V.; Cherniukh, I.; Nazarenko, O.; Kreil, D.; Nauser, T.; Kovalenko, M. V. *Nat. Photonics* **2016**, *10*, 585−589.
(25) Kepenekian, M.; Robles, R.; Katan, C.; Sapori, D.; Pedesseau, L.; Even, J. *ACS Nano* **2015**, *9*, 11557−11567.
(26) Yu, Z. G. *J. Phys. Chem. Lett.* **2016**, *7*, 3078−3083.
(27) Zhang, C.; Sun, D.; Sheng, C. X.; Zhai, Y. X.; Mielczarek, K.; Zakhidov, A.; Vardeny, Z. V. *Nat. Phys.* **2015**, *11*, 427−434.
(28) Hirasawa, M.; Ishihara, T.; Goto, T.; Uchida, K.; Miura, N. *Phys. B* **1994**, *201*, 427−430.
(29) Kim, M.; Im, J.; Freeman, A. J.; Ihm, J.; Jin, H. *Proc. Natl. Acad. Sci. U. S. A.* **2014**, *111*, 6900−6904.
(30) Zheng, F.; Tan, L. Z.; Liu, S.; Rappe, A. M. *Nano Lett.* **2015**, *15*, 7794−7800.
(31) Etienne, T.; Mosconi, E.; De Angelis, F. *J. Phys. Chem. Lett.* **2016**, *7*, 1638−1645.
(32) Manchon, A.; Koo, H. C.; Nitta, J.; Frolov, S. M.; Duine, R. A. *Nat. Mater.* **2015**, *14*, 871−882.
(33) Stroppa, A.; Di Sante, D.; Barone, P.; Bokdam, M.; Kresse, G.; Franchini, C.; Whangbo, M. H.; Picozzi, S. *Nat. Commun.* **2014**, *5*, 5900.
(34) Leppert, L.; Reyes-Lillo, S. E.; Neaton, J. B. *J. Phys. Chem. Lett.* **2016**, *7*, 3683−3689.
(35) Stoumpos, C. C.; Malliakas, C. D.; Peters, J. A.; Liu, Z.; Sebastian, M.; Im, J.; Chasapis, T. C.; Wibowo, A. C.; Chung, D. Y.; Freeman, A. J.; Wessels, B. W. *Cryst. Growth Des.* **2013**, *13*, 2722−2727.
(36) Stoumpos, C. C.; Kanatzidis, M. G. *Acc. Chem. Res.* **2015**, *48*, 2791−2802.
(37) Hoffman, J. B.; Schleper, A. L.; Kamat, P. V. *J. Am. Chem. Soc.* **2016**, *138*, 8603−8611.
(38) Comin, R.; Crawford, M. K.; Said, A. H.; Herron, N.; Guise, W. E.; Wang, X.; Whitfield, P. S.; Jain, A.; Gong, X.; McGaughey, l.J.H.; Sargent, E. H. *Phys. Rev. B: Condens. Matter Mater. Phys.* **2016**, *94*, 094301.
(39) Onoda-Yamamuro, N.; Matsuo, T.; Suga, H. *J. Phys. Chem. Solids* **1990**, *51*, 1383−1395.
(40) Onoda-Yamamuro, N.; Matsuo, T.; Suga, H. *J. Phys. Chem. Solids* **1992**, *53*, 935−939.
(41) Chen, Z.; Yu, C.; Shum, K.; Wang, J. J.; Pfenninger, W.; Vockic, N.; Midgley, J.; Kenney, J. T. *J. Lumin.* **2012**, *132*, 345−349.
(42) Wei, K.; Xu, Z.; Chen, R.; Zheng, X.; Cheng, X.; Jiang, T. *Opt. Lett.* **2016**, *41*, 3821−3824.
(43) Kong, W.; Ye, Z.; Qi, Z.; Zhang, B.; Wang, M.; Rahimi-Iman, A.; Wu, H. *Phys. Chem. Chem. Phys.* **2015**, *17*, 16405−16411.
(44) Gesi, K. *Ferroelectrics* **1997**, *203*, 249−268.
(45) Galkowski, K.; Mitioglu, A.; Surrente, A.; Yang, Z.; Maude, D. K.; Kossacki, P.; Eperon, G. E.; Wang, J.; Snaith, H. J.; Plochocka, P.; Nicholas, R. J. *Nanoscale* **2017**, *9*, 3222−3230.
(46) Löper, P.; Stuckelberger, M.; Niesen, B.; Werner, J.; Filipič, M.; Moon, S. J.; Yum, J. H.; Topič, M.; De Wolf, S.; Ballif, C. *J. Phys. Chem. Lett.* **2015**, *6*, 66−71.
(47) De Roo, J.; Ibanez, M.; Geiregat, P.; Nedelcu, G.; Walravens, W.; Maes, J.; Martins, J. C.; Van Driessche, I.; Kovalenko, M. V.; Hens, Z. *ACS Nano* **2016**, *10*, 2071−2081.
(48) Hsiao, Y. C.; Wu, T.; Li, M.; Liu, Q.; Qin, W.; Hu, B. *J. Mater. Chem. A* **2015**, *3*, 15372−15385.
(49) Stranks, S. D.; Eperon, G. E.; Grancini, G.; Menelaou, C.; Alcocer, M. J.; Leijtens, T.; Herz, L. M.; Petrozza, A.; Snaith, H. J. *Science* **2013**, *342*, 341−344.
(50) Xing, G.; Mathews, N.; Sun, S.; Lim, S. S.; Lam, Y. M.; Grätzel, M.; Mhaisalkar, S.; Sum, T. C. *Science* **2013**, *342*, 344−347.
(51) Yettapu, G. R.; Talukdar, D.; Sarkar, S.; Swarnkar, A.; Nag, A.; Ghosh, P.; Mandal, P. *Nano Lett.* **2016**, *16*, 4838−4848.
(52) Tanaka, K.; Takahashi, T.; Ban, T.; Kondo, T.; Uchida, K.; Miura, N. *Solid State Commun.* **2003**, *127*, 619−623.
(53) Tilchin, J.; Dirin, D. N.; Maikov, G. I.; Sashchiuk, A.; Kovalenko, M. V.; Lifshitz, E. *ACS Nano* **2016**, *10*, 6363−6371.
(54) Miyata, A.; Mitioglu, A.; Plochocka, P.; Portugall, O.; Wang, J. T. W.; Stranks, S. D.; Snaith, H. J.; Nicholas, R. J. *Nat. Phys.* **2015**, *11*, 582−587.
(55) Galkowski, K.; Mitioglu, A.; Miyata, A.; Plochocka, P.; Portugall, O.; Eperon, G. E.; Wang, J. T. W.; Stergiopoulos, T.; Stranks, S. D.; Snaith, H. J.; Nicholas, R. J. *Energy Environ. Sci.* **2016**, *9*, 962−970.
(56) Makarov, N. S.; Guo, S.; Isaienko, O.; Liu, W.; Robel, I.; Klimov, V. I. *Nano Lett.* **2016**, *16*, 2349−2362.

DOI: 10.1021/acs.nanolett.7b02248
Nano Lett. 2017, 17, 5020−5026

(57) Wu, X.; Trinh, M. T.; Niesner, D.; Zhu, H.; Norman, Z.; Owen, J. S.; Yaffe, O.; Kudisch, B. J.; Zhu, X. Y. *J. Am. Chem. Soc.* **2015**, *137*, 2089−2096.
(58) Sebastian, M.; Peters, J. A.; Stoumpos, C. C.; Im, J.; Kostina, S. S.; Liu, Z.; Kanatzidis, M. G.; Freeman, A. J.; Wessels, B. W. *Phys. Rev. B: Condens. Matter Mater. Phys.* **2015**, *92*, 235210.
(59) Endres, J.; Egger, D. A.; Kulbak, M.; Kerner, R. A.; Zhao, L.; Silver, S. H.; Hodes, G.; Rand, B. P.; Cahen, D.; Kronik, L.; Kahn, A. *J. Phys. Chem. Lett.* **2016**, *7*, 2722−2729.
(60) Even, J.; Pedesseau, L.; Katan, C. *J. Phys. Chem. C* **2014**, *118*, 11566−11572.
(61) Lang, L.; Yang, J. H.; Liu, H. R.; Xiang, H. J.; Gong, X. G. *Phys. Lett. A* **2014**, *378*, 290−293.
(62) Even, J.; Pedesseau, L.; Jancu, J. M.; Katan, C. *J. Phys. Chem. Lett.* **2013**, *4*, 2999−3005.
(63) Umebayashi, T.; Asai, K.; Kondo, T.; Nakao, A. *Phys. Rev. B: Condens. Matter Mater. Phys.* **2003**, *67*, 155405.
(64) Brivio, F.; Butler, K. T.; Walsh, A.; Van Schilfgaarde, M. *Phys. Rev. B: Condens. Matter Mater. Phys.* **2014**, *89*, 155204.
(65) Zhang, F.; Zhong, H.; Chen, C.; Wu, X.-G.; Hu, X.; Huang, H.; Han, J.; Zou, B.; Dong, Y. *ACS Nano* **2015**, *9*, 4533−4542.
(66) Tanaka, K.; Takahashi, T.; Kondo, T.; Umeda, K.; Ema, K.; Umebayashi, T.; Asai, K.; Uchida, K.; Miura, N. *Jpn. J. Appl. Phys.* **2005**, *44*, 5923−5932.
(67) Manser, J. S.; Christians, J. A.; Kamat, P. V. *Chem. Rev.* **2016**, *116*, 12956−13008.
(68) Yang, J.; Kelly, T. L. *Inorg. Chem.* **2017**, *56*, 92−101.
(69) Filip, M. R.; Eperon, G. E.; Snaith, H. J.; Giustino, F. *Nat. Commun.* **2014**, *5*, 5757.
(70) Stroppa, A.; Quarti, C.; De Angelis, F.; Picozzi, S. *J. Phys. Chem. Lett.* **2015**, *6*, 2223−2231.
(71) Liu, S.; Zheng, F.; Grinberg, I.; Rappe, A. M. *J. Phys. Chem. Lett.* **2016**, *7*, 1460−1465.
(72) Leguy, A. M.; Frost, J. M.; McMahon, A. P.; Sakai, V. G.; Kockelmann, W.; Law, C.; Li, X.; Foglia, F.; Walsh, A.; O'regan, B. C.; Nelson, J. *Nat. Commun.* **2015**, *6*, 7124.
(73) Stoumpos, C. C.; Malliakas, C. D.; Kanatzidis, M. G. *Inorg. Chem.* **2013**, *52*, 9019−9038.
(74) Weller, M. T.; Weber, O. J.; Henry, P. F.; Di Pumpo, A. M.; Hansen, T. C. *Chem. Commun.* **2015**, *51*, 4180−4183.
(75) Poglitsch, A.; Weber, D. *J. Chem. Phys.* **1987**, *87*, 6373−6378.
(76) Bakulin, A. A.; Selig, O.; Bakker, H. J.; Rezus, Y. L.; Müller, C.; Glaser, T.; Lovrincic, R.; Sun, Z.; Chen, Z.; Walsh, A.; Frost, J. M. *J. Phys. Chem. Lett.* **2015**, *6*, 3663−3669.
(77) Frost, J. M.; Butler, K. T.; Brivio, F.; Hendon, C. H.; Van Schilfgaarde, M.; Walsh, A. *Nano Lett.* **2014**, *14*, 2584−2590.
(78) Yaffe, O.; Guo, Y.; Tan, L. Z.; Egger, D. A.; Hull, T.; Stoumpos, C. C.; Zheng, F.; Heinz, T. F.; Kronik, L.; Kanatzidis, M. G.; Owen, J. S. *Phys. Rev. Lett.* **2017**, *118*, 136001.
(79) Fabini, D. H.; Laurita, G.; Bechtel, J. S.; Stoumpos, C. C.; Evans, H. A.; Kontos, A. G.; Raptis, Y. S.; Falaras, P.; Van der Ven, A.; Kanatzidis, M. G.; Seshadri, R. *J. Am. Chem. Soc.* **2016**, *138*, 11820−11832.
(80) Bertolotti, F.; Dirin, D. N.; Ibáñez, M.; Krumeich, F.; Cervellino, A.; Frison, R.; Voznyy, O.; Sargent, E. H.; Kovalenko, M. V.; Guagliardi, A.; Masciocchi, N. *Nat. Mater.* **2016**, *15*, 987−994.
(81) Bychkov, Y. A.; Rashba, E. I. *JETP Lett.* **1984**, *39*, 78−81.
(82) Ganichev, S. D.; Golub, L. E. *Phys. Status Solidi B* **2014**, *251*, 1801−1823.
(83) Rashba, E. I.; Sherman, E. Y. *Phys. Lett. A* **1988**, *129*, 175−179.
(84) Dresselhaus, G. *Phys. Rev.* **1955**, *100*, 580−586.
(85) Yu, Z. G. *J. Phys. Chem. Lett.* **2016**, *7*, 3078−3083.
(86) Niesner, D.; Wilhelm, M.; Levchuk, I.; Osvet, A.; Shrestha, S.; Batentschuk, M.; Brabec, C.; Fauster, T. *Phys. Rev. Lett.* **2016**, *117*, 126401.
(87) Berhe, T. A.; Su, W. N.; Chen, C. H.; Pan, C. J.; Cheng, J. H.; Chen, H. M.; Tsai, M. C.; Chen, L. Y.; Dubale, A. A.; Hwang, B. J. *Energy Environ. Sci.* **2016**, *9*, 323−356.
(88) Tong, Y.; Bladt, E.; Aygüler, M. F.; Manzi, A.; Milowska, K. Z.; Hintermayr, V. A.; Docampo, P.; Bals, S.; Urban, A. S.; Polavarapu, L.; Feldmann, J. *Angew. Chem., Int. Ed.* **2016**, *55*, 13887−13892.
(89) Hintermayr, V. A.; Richter, A. F.; Ehrat, F.; Döblinger, M.; Vanderlinden, W.; Sichert, J. A.; Tong, Y.; Polavarapu, L.; Feldmann, J.; Urban, A. S. *Adv. Mater.* **2016**, *28*, 9478−9485.
(90) Bertolotti, F.; Protesescu, L.; Kovalenko, M. V.; Yakunin, S.; Cervellino, A.; Billinge, S. J.; Terban, M. W.; Pedersen, J. S.; Masciocchi, N.; Guagliardi, A. *ACS Nano* **2017**, *11*, 3819−3831.
(91) Korona, K. P.; Wysmol, A.; Pakul, K.; Stepniewski, R.; Baranowski, J. M.; Grzegory, I.; Wroblewski, M.; Porowski, S. *Appl. Phys. Lett.* **1996**, *69*, 788−790.
(92) Wright, A. D.; Verdi, C.; Milot, R. L.; Eperon, G. E.; Pérez-Osorio, M. A.; Snaith, H. J.; Giustino, F.; Johnston, M. B.; Herz, L. M. *Nat. Commun.* **2016**, *7*, 11755.
(93) Yanover, D.; Čapek, R. K.; Rubin-Brusilovski, A.; Vaxenburg, R.; Grumbach, N.; Maikov, G. I.; Solomeshch, O.; Sashchiuk, A.; Lifshitz, E. *Chem. Mater.* **2012**, *24*, 4417−4423.
(94) Fu, M.; Tamarat, P.; Huang, H.; Even, J.; Rogach, A. L.; Lounis, B. *Nano Lett.* **2017**, *17*, 2895−2901.
(95) Van Bree, J.; Silov, A. Y.; Koenraad, P. M.; Flatté, M. E.; Pryor, C. E. *Phys. Rev. B: Condens. Matter Mater. Phys.* **2012**, *85*, 165323.
(96) Jovanov, V.; Eissfeller, T.; Kapfinger, S.; Clark, E. C.; Klotz, F.; Bichler, M.; Keizer, J. G.; Koenraad, P. M.; Brandt, M. S.; Abstreiter, G.; Finley, J. J. *Phys. Rev. B: Condens. Matter Mater. Phys.* **2012**, *85*, 165433.
(97) Kuok, M. H.; Tan, L. S.; Shen, Z. X.; Huan, C. H.; Mok, K. F. *Solid State Commun.* **1996**, *97*, 497−501.
(98) Hirotsu, S. *Phys. Lett. A* **1972**, *41*, 55−56.

DOI: 10.1021/acs.nanolett.7b02248
Nano Lett. 2017, 17, 5020−5026